SUPPLEMENTARY INFORMATION

August 5, 2022

Mapping Simulated Two-Dimensional Spectra to Molecular Models Using Machine Learning

Kelsey A. Parker,† Jonathan D. Schultz,‡ Niven Singh,¶ Michael R. Wasielewski,*,‡ and David N. Beratan,*,†,§,‖
†*Department of Chemistry, Duke University, Durham, NC 27708, USA*
‡*Department of Chemistry and Institute for Sustainability and Energy, Northwestern University, Evanston, IL 60208-3113, USA*
¶*Program in Computational Biology and Bioinformatics, Center for Genomics and Computational Biology, Duke University School of Medicine, Durham, NC 27710, USA*
§*Department of Biochemistry, Duke University, Durham, NC 27710, USA*
‖*Department of Physics, Duke University, Durham, NC 27708, USA*

TABLE OF CONTENTS

Section S1. Feedforward Neural Networks [Fig. S1, Eqs. S1-S5]

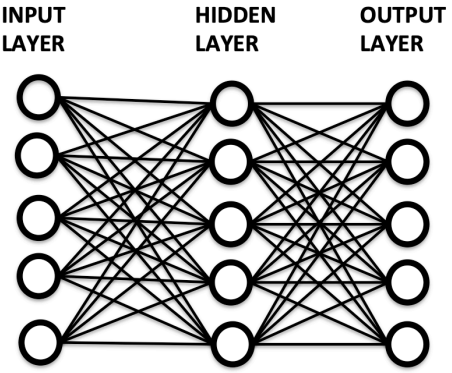

Figure S1. A feedforward neural network including the input, hidden, and output layers with neurons (circles) and activation functions (lines)

This study used a simple feedforward neural network (NN), like the one shown in Fig. S1. In this diagram, the circles represent neurons. The layer of neurons on the far left, called the input layer, is made up of the input numbers; in this study, these values describe the 2D spectra. The neurons in the middle layer, called the hidden layer, and the neurons in the far right layer, called the output layer, depend on the neurons in the previous layer according to Equation S1,

$$a_j^{[l]} = \sigma\left(\sum_k w_{jk}^{[l]} a_k^{[l-1]} - b_j^{[l]}\right) \quad \text{S1}$$

where $a_j^{[l]}$ is the value of the jth neuron in the lth layer and $a_k^{[l-1]}$ is the value of the kth neuron from the previous layer. The terms $w_{jk}^{[l]}$ and $b_j^{[l]}$ are called weights and biases, respectively. The subscripts for these terms are indexes describing the neurons involved and the superscripts indicate the layer in the NN. The weights and biases are initialized randomly and change during training. The summation goes over all the neurons in the previous layer. The term, σ, is an activation function.[1] In this study, the activation function between the hidden and output layers is linear. We considered two activation functions between the input and hidden layers called the rectified linear unit (ReLU)[2-4] and the Leaky ReLU,[5] shown below in Equations S2 and S3 respectively.

$$\sigma_{ReLU}(\chi) = \begin{cases} \chi, & \text{if } \chi > 0 \\ 0, & \text{otherwise} \end{cases} \quad \text{S2}$$

$$\sigma_{Leaky\ ReLU}(\chi) = \begin{cases} \chi, & \text{if } \chi > 0 \\ 0.01\chi, & \text{otherwise} \end{cases} \quad \text{S3}$$

The values of the neurons at the output layer are put into a cost function like that shown in Equation S4. The term, $\boldsymbol{a}^{(L)}(\boldsymbol{x}^{(1)})$ includes the initial input, $(\boldsymbol{x}^{(1)})$, and returns the output from the final layer of the NN with number of layers, L. The known output corresponding to an input of $(\boldsymbol{x}^{(1)})$ is $\boldsymbol{y}(\boldsymbol{x}^{(1)})$; the superscript in Equation S4 indicates that the values are for a single input and corresponding output. By comparing the output from the NN with the true value, this equation is measuring the accuracy of the NN.

$$C(\boldsymbol{x}^{(1)}) = \frac{1}{2}\left\|\boldsymbol{y}(\boldsymbol{x}^{(1)}) - \boldsymbol{a}^{(L)}(\boldsymbol{x}^{(1)})\right\|^2 \quad \text{S4}$$

In Equation S5, the cost function is expanded to include a large set of inputs and their corresponding, known outputs. The multiple in front of the sum in Eq. S5 includes the number of all inputs and outputs in the set, *X*. Using the chain rule, the weights and biases can be systematically improved to minimize this cost function via gradient descent. This process is called training the NN. After training, the NN with the finalized set of weights and biases is tested to determine its applicability to the given problem.[1]

$$C(\boldsymbol{x}) = \frac{1}{2X}\left\|\boldsymbol{y}(\boldsymbol{x}) - \boldsymbol{a}^{(L)}(\boldsymbol{x})\right\|^2 \quad \text{S5}$$

Section S2. Spectral Simulations [Table S1]

All calculations in this work are formulated within the Condon and harmonic approximations. For each vibration *m* included in Equation (1), we account for a maximum of five excited vibrational quanta and assume that the site-basis vibrational frequency is constant across all electronic states and molecules (in the case of a dimer). Our simulations of the third-order response functions are performed entirely within a time-domain representation, as has been employed in many previous works.[6,7] Here, we calculate the third-order absorptive response $\left(R_{abs}^{(3)}(t_1, t_2, t_3)\right)$ as the sum of the real rephasing and non-rephasing signals, which both contain ground-state bleach and stimulated emission responses. Fast Fourier transformation (FFT) of $\left(R_{abs}^{(3)}(t_1, t_2, t_3)\right)$ with respect to t_1, which is the time delay between the two pump light-matter interactions, yields the excitation frequency (ω_1) resolution. Likewise, we FFT along t_3 (the delay between the probe pulse and signal emission event) to obtain resolution in the detection frequency axis (ω_3). Therefore, absorptive signals used as inputs to the NN are of mixed frequency- and time-domain representation $\left(R_{abs}^{(3)}(\omega_1, t_2, \omega_3)\right)$. Spectral linewidths were captured by multiplying $R_{abs}^{(3)}(t_1, t_2, t_3)$ by a lineshape function that accounts for energy gap fluctuations (ΔE) and a correlation timescale (t_c).[8] Table S1 summarizes these parameters as well as additional values pertaining specifically to time-simulation of $R_{abs}^{(3)}(t_1, t_2, t_3)$.

Table S1. Phenomenological system-bath parameters and metrics for time-domain simulations used to produce the theoretical 2DES spectra in this study. These values were held constant for all simulations.

Parameter	t_1, t_3 domains	t_2 domain
ΔE	1200 cm^{-1}	50 cm^{-1}
t_c	40 fs	300 fs
step size (Δt)	3 fs	30 fs
initial time	0 fs	0 fs
final time	186 fs	1500 fs

As shown in Table S1, $R_{abs}^{(3)}(t_1, t_2, t_3)$ was calculated from 0 to 186 fs along the t_1 and t_3 domains with a step size of 3 fs. Without zero padding, this translates to a frequency resolution of approximately 176 cm^{-1} for both the ω_1 and ω_3 axes. Prior to Fourier transformation of the data along the t_1 and t_3 dimensions, we zero padded the data by a factor of four. Since zero padding by a factor of two improves resolution by accounting for causality,[9] the effective frequency resolution along ω_1 and ω_3 is approximately 88 cm^{-1}.

As most of the molecular response occurs within a relatively small fraction of the total frequency range (ω_1, ω_3), we cut the 2D spectra down to a window of 5000 cm^{-1} in both ω_1 and ω_3 dimensions prior to proceeding with NN analyses. This window was automatically centered at the (ω_1, ω_3) coordinates of the maximum signal plus one quantum of the highest-frequency vibration present. In cases where the 0-0 vibronic band did not correspond to the highest signal intensity (i.e., for dimers with J ≥ 400 cm^{-1} and monomers with $\lambda = 1$ for the high-frequency vibration), we recentered this window in both ω_1 and ω_3 dimensions to the energy of the electronic energy gap (ε in Eq. 1) plus one quantum of the highest-frequency vibration present. This cutting process kept the inputs to the NN tractable in size while preserving the majority of the signal within the viewing window, which in turn also removes any physical meaning in absolute shifts in the signal along ω_1 and ω_3.

Section S3. Image Modifications [Fig. S2]

For each model Hamiltonian, the simulated spectral dataset is a 3D array of size: $n_{\omega_3}, n_{\omega_1}, n_{t_2}$ where n_{t_2} is the number of waiting times considered, n_{ω_1} is the number of data points along the excitation axis, and n_{ω_3} is the number of data points along the emission axis. As stated in the manuscript, $n_{t_2} = 51$, since spectra were collected at 30 fs intervals from 0 to 1500 fs. n_{ω_1} and n_{ω_3} were equal and always either 114 or 113, due to variation in how the axes of 2DES spectra were cut.

Prior to running the NNs, the 2D spectra were modified using an in-house trimming and resizing script. The main purpose of these modifications was to insure the input layer was the same size for all spectra (as some spectra had 114*114 data points while others had 113*113 data points) and to cut down on the size of the input layer. Prior to trimming, the images were re-centered to give the most even distribution of $R_{abs}^{(3)}$ magnitudes around the new ω_1 and ω_3 center coordinates. The images were then cut to contain ~95% and ~90% of the total amount of $R_{abs}^{(3)}$ magnitudes. Images were also left unchanged by the trimming script ('no trim' in the manuscript). The images were then resized to arrays of size: 40*40, 50*50, and 60*60. This resizing was accomplished with a bilinear interpolation script that averaged $R_{abs}^{(3)}$ values across the ω_1 and ω_3 indices.

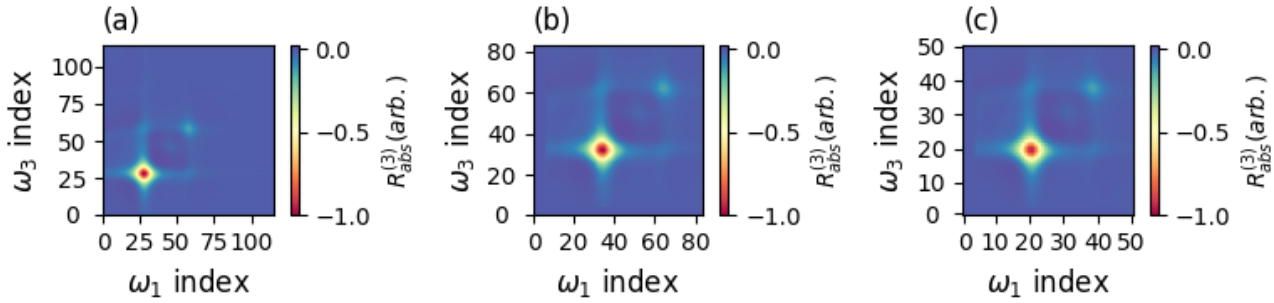

Figure S2. 2D spectrum from a monomer at $t_2 = 0\ fs$ with high- and mid- frequency modes with λ values of 0.35 and 0.25, respectively (a) before image modifications, (b) after re-centering the image and trimming to 90%, and (c) after resizing the trimmed image to have 50*50 data points.

An example of the trimming and resizing process is shown in Fig. S2. Figure S2(a) is the original spectrum; the original image has 114 points along ω_1 and ω_3. Figure S2(b) is the image after re-centering and trimming to ~90%; the image now has 83 points along ω_1 and ω_3. Finally, Fig. S2(c) is the image following resizing to contain 50 points along ω_1 and ω_3.

Section S4. Number of Epochs and Learning Curves

To determine the number of epochs to use while optimizing the hyperparameters in this study, we did preliminary training and testing runs at various hyperparameter combinations. We found that using 100 epochs resulted in training learning curves that decreased monotonically and stabilized at low loss values while also returning high accuracy values for the test set. 100 epochs was also computationally affordable. Figure S3 shows example learning curves for training a NN for Question 5 along with corresponding accuracy values for the test set at each epoch. The training learning curve, Fig. S3(a) has more points compared to the test accuracy curve, Fig. S3(b) because we printed the loss value several times while training with minibatches. As shown in Fig. S3(a), the loss while training drops rapidly and stabilizes close to 0 after ~50 epochs. In Fig. S3(b), the accuracy of the test set increases and stays above 90% after ~30 epochs.

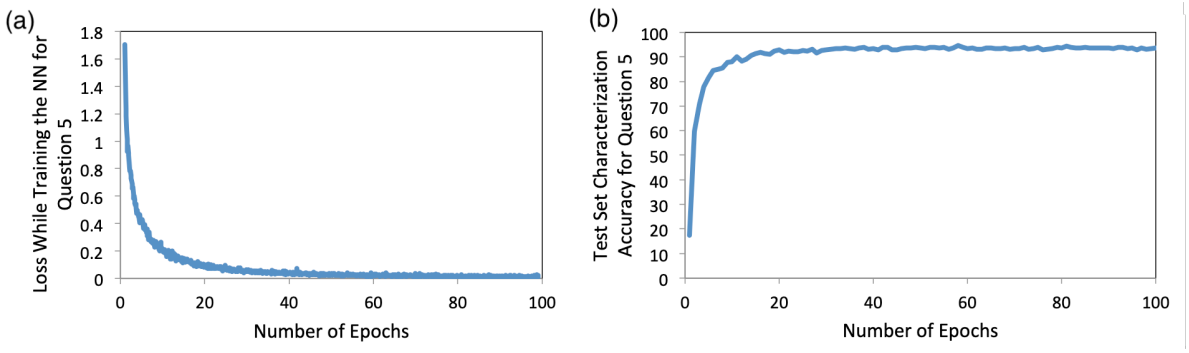

Figure S3. (a) An example learning curve from training for Question 5 showing the loss vs. epochs and (b) the corresponding accuracy values generated for the test set at each epoch; the hyperparameters are: spectra trimming = none, input size = 3600, neurons in hidden layer = 500, activation function = ReLU, batch size = 500, learning rate = 0.001.

Section S5. References

1. Nielsen, M. A. *Neural networks and deep learning;* Determination press: San Francisco, CA, USA, 2015, *25*.
2. Fukushima, K. Neocognition: a Self-organizing Neural Network Model for a Mechanism of Pattern Recognition Unaffected by Shift in Position. *Biol. Cybern.* **1980**, *36*, 193-202.
3. Rumelhart, D. E.; Hinton, G. E; McClelland, J. L., et al. *Parallel distributed processing: Explorations in the Microstructure of Cognition*. MIT Press: Cambridge, MA, USA, 1986.
4. Nair, V; Hinton, G. E. Rectified Linear Units Improve Restricted Boltzmann Machines. *In Proc. International Conference on Machine Learning*, 2010, 807-814.
5. Maas, A. L. Hannun, A. Y.; Ng, A. Y. Rectifier Nonlinearities Improve Neural Network Acoustic Models. *In Proc. International Conference on Machine Learning*, 2013, 3-8.
6. Halpin, A.; Johnson, P. J.; Tempelaar, R.; Murphy, R. S.; Knoester, J.; Jansen, T. L.; Miller, R. D. Two-dimensional Spectroscopy of a Molecular Dimer Unveils the Effects of Vibronic Coupling on Exciton Coherences. *Nat. Chem.* **2014**, *6*, 196-201.
7. Tempelaar, R.; Jansen, T. L.; Knoester, J. Vibrational Beatings Conceal Evidence of Electronic Coherence in the FMO Light-Harvesting Complex. *J. Phys. Chem. B* **2014**, *118*, 12865-12872.
8. Kubo, R.; *Fluctuation, Relaxation, and Resonance in Magnetic Systems*. Oliver and Boyd Ltd: London, UK, 1962.
9. Hamm, P; Zanni, M. *Concepts and methods of 2D infrared spectroscopy*. Cambridge University Press: Cambridge, UK, 2011.